7
Bibliografia

1. GOUVÊA, P. M. P. et al. Internal Specular Reflection from Nanoparticle Layers on the End Face of Optical Fibers. **Journal of Applied Physics**, 109, 2011. 103114.
2. DAL LAGO, V. et al. Size-selective silver nanoparticles: future of biomedical devices with enhanced bactericidal properties. **Journal of Materials Chemistry**, 21, 2011. 12267 – 12273.
3. FÁVERO, F. C. Sensores a Fibras Ópticas Microestruturadas, Rio de Janeiro, Março 2012. http://www2.dbd.puc-rio.br/pergamum/tesesabertas.
4. FAVERO, F. C. et al. Spheroidal Fabry-Perot microcavities in optical fibers for high-sensitivity sensing. **Optics Express**, 7, 2012. 7112 – 7118.
5. MARKOS, P.; SOUKOULIS, C. M. **Wave Propagation**. Princeton: Princeton University Press, 2008.
6. BOHREN, C. F.; HUFFMAN, D. R. **Absorption and Scattering of Light by Small Particles**. New York: Wiley - VCH, 1998. 544 p. ISBN 9780471293408.
7. FONTANA, J. P. Self-assembly and Characterization of Anisotropic Metamaterials, 29 Março 2011. http://www.e-lc.org/dissertations/.
8. KELLY, K. L. et al. The Optical Properties of Metal Nanoparticles: The Influence of Size, Shape, and Dielectric Environment. **J. Physical Chemistry B**, 107, n. 3, 2003. 668 – 677.
9. KALKVRENNER, T.; ULF, H.; SANDOGHDAR, V. Tomographic Plasmon Spectroscopy of a Single Gold Nanoparticle. **Nano Latters**, 4, n. 12, 2004. 2309 – 2314.
10. ROMANI, E. C. et al. Gold nanoparticleson on the surface of soda-lime glass. **Optics Express**, 20, n. 5, 2012. 5429 – 5439.
11. JACKSON, J. D. **Classical Electrodynamics**. 3ª Edição. ed. New York: Wiley - VCH, 1998. 832 p. ISBN 9780471309321.
12. PEDROSO, C. B. Propriedades Ópticas de Materiais Compostos: Modelo de Maxwell-Garnett e Modelo de Lorentz, Campinas, 29 Outubro 1993.
13. MERIAUDEAU, F. et al. Fiber Optic Sensor Based on Gold Island Plasmon Resonance. **Sensors and Actuators B**, 54, 1999. 106 – 117.
14. LIN, T.-J.; LOU, C.-T. Reflection-Based Localized Surface Plasmon Resonance Fiber-Optic Probe. **Journal of Supercritical Fluids**, 41, 2001. 317 – 325.
15. ANDRADE, G. F. S.; FAN, M.; BROLO, A. G. Multilayer Silver Nanoparticles-Modified Optical Fiber Tip for High Performance SERS Remote Sensing. **Biosensors and Bioelectronics**, 25, 2010. 2270 – 2275.

16. YOSHINO, T. et al. Fiber-optic Fabry-Perot Interferometer and its Sensor Applications. **IEEE Journal of Quantum Electronics**, 30, 1982. 1612 – 1621.
17. HECHT, E. **Optics**. 2ª. ed. Reading: Addison-Wesley, 1987. ISBN 0201116111.
18. KUMARI, G.; NARAYANA, C. New Nano Architecture for SERS Applications. **Journal of Physical Chemistry Letters**, 2012. 1130 – 1135.

8
Anexo: Artigo Publicado em Periódico Internacional

F. C. Favero, L. Araujo, G. Bouwmans, V. Finazzi, J. Villatoro e V. Pruneri, "Spheroidal Fabry-Perot microcavities in optical fibers for high-sensitivity sensing", Optics Express, vol. 20, nº. 7 (2012).

Spheroidal Fabry-Perot microcavities in optical fibers for high-sensitivity sensing

F. C. Favero,[1,2] L. Araujo,[1] G. Bouwmans,[3] V. Finazzi,[2] J. Villatoro,[2,*] and V. Pruneri[2,4]

[1]*Pontifical Catholic University of Rio de Janeiro, Rua Marquês de São Vicente 225, 22453-900, Rio de Janeiro, RJ, Brazil*

[2]*ICFO- Institut de Ciencies Fotoniques, Mediterranean Technology Park, 08860, Castelldefels, Barcelona, Spain*

[3]*PhLAM/IRCICA, Université Lille, CNRS UMR8523/USR3380, 59658 Villeneuve d'Ascq, France*

[4]*Also with ICREA-Institució Catalana de Recerca i Estudis Avançats, 08010, Barcelona, Spain*

[*] *joel.villatoro@icfo.es*

Abstract: All-optical-fiber Fabry-Perot interferometers (FPIs) with microcavities of different shapes were investigated. It was found that the size and shape of the cavity plays an important role on the performance of these interferometers. To corroborate the analysis, FPIs with spheroidal cavities were fabricated by splicing a photonic crystal fiber (PCF) with large voids and a conventional single mode fiber (SMF), using an ad hoc splicing program. It was found that the strain sensitivity of FPIs with spheroidal cavities can be controlled through the dimensions of the spheroid. For example, a FPI whose cavity had a size of ~10x60 μm exhibited strain sensitivity of ~10.3 pm/με and fringe contrast of ~38 dB. Such strain sensitivity is ~10 times larger than that of the popular fiber Bragg gratings (~1.2 pm/με) and higher than that of most low-finesse FPIs. The thermal sensitivity of our FPIs is extremely low (~1pm/°C) due to the air cavities. Thus, a number of temperature-independent ultra-sensitive microscopic sensors can be devised with the interferometers here proposed since many parameters can be converted to strain. To this end, simple vibration sensors are demonstrated.

OCIS codes: (060.2370) Fiber optics sensors; (060.5295) Photonic crystal fibers; (280.4788) Optical sensing and sensors; (120.2230) Fabry-Perot; (120.3180) Interferometry.

References and links

1. Y.-J. Rao, "Recent progress in fiber-optic extrinsic Fabry–Perot interferometric sensors," Opt. Fiber Technol. **12**(3), 227–237 (2006).
2. J.-H. Chen, X.-G. Huang, and Z.-J. Huang, "Simple thin-film fiber optic temperature sensor based on Fabry-Perot interference," Opt. Eng. **49**(4), 044402 (2010).
3. C. Lee, L. Lee, H. Hwang, and J. Hsu, "Highly sensitive air-gap fiber Fabry-Perot interferometers based on polymer-filled hollow core fibers," IEEE Photon. Technol. Lett. **24**(2), 149–151 (2012).
4. N. V. Wheeler, M. D. W. Grogan, T. D. Bradley, F. Couny, T. A. Birks, and F. Benabid, "Multipass hollow core-pcf microcell using a tapered micromirror," J. Lightwave Technol. **29**(9), 1314–1318 (2011).
5. S. Pevec and D. Donlagic, "All-fiber, long-active-length Fabry-Perot strain sensor," Opt. Express **19**(16), 15641–15651 (2011).
6. C. Tuck, R. Hague, and C. Doyle, "Low cost optical fibre based Fabry–Perot strain sensor production," Meas. Sci. Technol. **17**(8), 2206–2212 (2006).
7. X. Chen, F. Shen, Z. Wang, Z. Huang, and A. Wang, "Micro-air-gap based intrinsic Fabry-Perot interferometric fiber-optic sensor," Appl. Opt. **45**(30), 7760–7766 (2006).
8. E. Cibula and D. Donlagic, "In-line short cavity Fabry-Perot strain sensor for quasi distributed measurement utilizing standard OTDR," Opt. Express **15**(14), 8719–8730 (2007).
9. Y.-J. Rao, M. Deng, D.-W. Duan, X.-C. Yang, T. Zhu, and G.-H. Cheng, "Micro Fabry-Perot interferometers in silica fibers machined by femtosecond laser," Opt. Express **15**(21), 14123–14128 (2007).
10. T. Wei, Y. Han, Y. Li, H.-L. Tsai, and H. Xiao, "Temperature-insensitive miniaturized fiber inline Fabry-Perot interferometer for highly sensitive refractive index measurement," Opt. Express **16**(8), 5764–5769 (2008).
11. J. Sirkis, T. A. Berkoff, R. T. Jones, H. Singh, A. D. Kersey, E. J. Friebele, and M. A. Putnam, "In-Line fiber etalon (ILFE) fiber-optic strain sensors," J. Lightwave Technol. **13**(7), 1256–1263 (1995).
12. Y. J. Rao, T. Zhu, X. C. Yang, and D. W. Duan, "In-line fiber-optic etalon formed by hollow-core photonic crystal fiber," Opt. Lett. **32**(18), 2662–2664 (2007).

#162708 - $15.00 USD Received 8 Feb 2012; revised 7 Mar 2012; accepted 8 Mar 2012; published 13 Mar 2012

13. Q. Shi, Z. Wang, L. Jin, Y. Li, H. Zhang, F. Lu, G. Kai, and X. Dong, "A hollow-core photonic crystal fiber cavity based multiplexed Fabry–Pérot interferometric strain sensor system," IEEE Photon. Technol. Lett. 20(15), 1329–1331 (2008).
14. E. Li, G. D. Peng, and X. Ding, "High spatial resolution fiber-optic Fizeau interferometric strain sensor based on an in-fiber spherical microcavity," Appl. Phys. Lett. 92(10), 101117 (2008).
15. J. Villatoro, V. Finazzi, G. Coviello, and V. Pruneri, "Photonic-crystal-fiber-enabled micro-Fabry-Perot interferometer," Opt. Lett. 34(16), 2441–2443 (2009).
16. F. C. Favero, G. Bouwmans, V. Finazzi, J. Villatoro, and V. Pruneri, "Fabry-Perot interferometers built by photonic crystal fiber pressurization during fusion splicing," Opt. Lett. 36(21), 4191–4193 (2011).
17. A. D. Kersey, M. A. Davis, H. J. Patrick, M. LeBlanc, K. P. Koo, C. G. Askins, M. A. Putnam, and E. J. Friebele, "Fiber grating sensors," J. Lightwave Technol. 15(8), 1442–1463 (1997).
18. A. Laudati, F. Mennella, M. Giordano, G. D'Altrui, C. Calisti Tassini, and A. Cusano, "A fiber-optic Bragg grating seismic sensor," IEEE Photon. Technol. Lett. 19(24), 1991–1993 (2007).
19. T. Guo, A. Ivanov, C. Chen, and J. Albert, "Temperature-independent tilted fiber grating vibration sensor based on cladding-core recoupling," Opt. Lett. 33(9), 1004–1006 (2008).
20. M. Kamata, M. Obara, R. R. Gattass, L. R. Cerami, and E. Mazur, "Optical vibration sensor fabricated by femtosecond laser micromachining," Appl. Phys. Lett. 87(5), 051106 (2005).
21. T. Ke, T. Zhu, Y. J. Rao, and M. Deng, "Accelerometer based on all-fiber Fabry-Perot interferometer formed by hollow-core photonic crystal fiber," Microw. Opt. Technol. Lett. 52(11), 2531–2535 (2010).

1. Introduction

The Fabry-Perot interferometer (FPI) is one of the most versatile interferometers since it can be implemented in many different ways, see for example [1]. In its simplest configuration the quoted interferometer can be implemented with Fresnel reflections from two air-glass or glass-dielectric interfaces separated by a microscopic distance [2–5]. To avoid alignment elements and minimize the fabrication steps, monolithic fiber FPIs have been proposed in which a cavity is made by means of chemical etching [6–8], femto-second laser machining [9,10], or by inserting a short segment of hollow fiber or tube between optical fibers [11–13]. Another possibility to make alignment-free FPIs is by fusion splicing a photonic crystal fiber (PCF) and a standard optical fiber together [14–16]. All the aforementioned FPIs can be good choices for optical sensing since a minute change of the cavity size or index leads to a detectable shift of the interference pattern. The sensitivities achieved with most low-finesse FPIs reported until now are comparable to that of the popular fiber Bragg gratings (FBG). To the authors' best knowledge, no mechanism to enhance the sensitivity of FPIs while keeping their main advantages (microscopic size, robustness, minimal fabrication steps, etc.) has been proposed so far.

Here, we show that the shape and dimensions of the cavity help to substantially enhance the performance of a fiber FPI. Interferometers with cavities of spherical and spheroidal shapes are analyzed theoretically but the analysis of interferometers with cavities of other shapes is straightforward. We demonstrate a FPI with spheroidal cavity of size ~10x60 μm that exhibited fringe contrast of 38 dB (visibility of 0.99984). We believe that such visibility is the highest one ever reported for a low-finesse FPI. In addition to the high visibility, the referred device exhibited a strain sensitivity of ~10.3 pm/με which is ~10 times higher than that of the popular FBG (~1.2pm/με) [17] and higher than that of most low-finesse FPIs previously reported. To achieve FPIs with spheroidal cavities we fusion spliced a properly-selected PCF to a single mode optical fiber (SMF) with an on-purpose splicing program.

2. Theoretical analysis

Let us assume a FPI whose cavity is made of air, has quasi-spherical ($r \approx d$) or spheroidal shape and that is completed embedded in an optical fiber whose diameter is $2R$, see Fig. 1. In

#162708 - $15.00 USD Received 8 Feb 2012; revised 7 Mar 2012; accepted 8 Mar 2012; published 13 Mar 2012

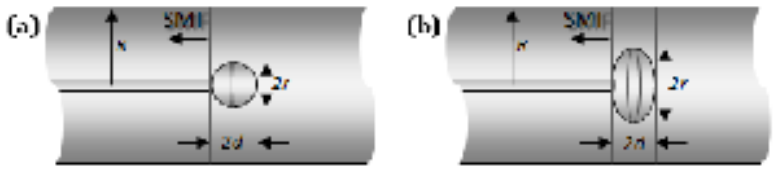

Fig. 1. Diagram of a Fabry-Perot interferometer with (a) spherical and (b) spheroidal air cavities which are assumed to be at the end of a single mode fiber (SMF), in front of its core.

the following analysis an oblate spheroid, *i.e.*, an ellipse rotated around its minor axis, with size of $2d$x$2r$ ($r > d$) will be assumed, where $2d$ is the polar diameter and r the equator radius. Note that the spheroid polar axis (equator plane) is assumed to coincide with the direction of light propagation. Light reflected from the SMF-air interface and that reflected from the air-glass interface can be coupled back into the SMF and interfere. The accumulated phase difference between the two Fresnel reflections is $\varphi \approx 4\pi nd/\lambda + \pi$, where λ is the wavelength of the optical source and n the refractive index of the medium inside the cavity. Thus, if one launches light from a broadband source to the cavity and the reflection is analyzed with a spectrometer a series of maxima and minima (interference pattern) can be expected. The maxima will appear whenever $\varphi = 2\pi m$, with m a strictly positive integer. This means, at wavelengths that satisfy the condition: $\lambda_m = 2nd/(m-1/2)$.

Like a FPI with flat reflecting surfaces, a FPI with spherical or spheroidal cavity can be used for sensing physical parameters such as strain ($\delta d/d$) and any other parameter that can be transduced to strain, *e.g.*, pressure, load, vibration, tilt, etc. Any of these parameters will induce solely a minute change of the cavity size since the cavity is assumed to be made of air ($n = 1$). The changes experienced by the interferometer cavity will result in a shift in the position of the interference maxima (or minima) by $\delta\lambda_m$. To correlate the shift of the interference pattern with the change of the cavity size hence to estimate the sensitivity, it is necessary to differentiate λ_m. This leads to the simple expression: $\delta\lambda_m = \lambda_m(\delta d/d)$. Most authors assume that the strain sensitivity of a FPI is independent of the cavity size and that it can be enhanced solely by choosing longer wavelengths. Recent results reported by our group in [15] and [16] suggest that the cavity size and shape of a FPI plays an important role in the interferometer performance and motivated the work here presented.

If a FPI with cavities like those described in Fig. 1 is subjected to axial strain, force or pressure it will experience the so-called Poisson effect which states that if d changes by δd then r will change by δr. Thus, an axial strain ($\varepsilon_a = \delta d/d$) applied to the cavity will induce a transversal strain ($\varepsilon_t = \delta r/r$) to the same. The axial and the transversal strains are related to each other by means of the Poisson's ratio ($\nu = -\varepsilon_t/\varepsilon_a$). Thus, the shift of the interference pattern of a FPI with quasi-spherical or spheroidal cavity depends on ν which in turn is proportional to $dr/\delta d$. To calculate the Poisson's ratio we need to analyze the volume (V) of the section of optical fiber that contains the cavity and its microscopic changes (δV). If δV is caused for example by changes of pressure and temperature, then the following expression is fulfilled:

$$\frac{\delta V}{V} = \frac{-1}{K}\delta P + \gamma\delta T. \qquad (1)$$

In Eq. (1), K is the bulk modulus and γ is the coefficient of thermal expansion. Let us assume that the change in pressure is due to axial strain applied to the optical fiber. Thus, pressure and strain are related by means of the Young's modulus $E = \sigma/\varepsilon_a = \delta P/\varepsilon_a$ (where σ is the tensile stress and ε_a is the axial strain). The volumetric changes caused by temperature can be

#162708 - $15.00 USD Received 8 Feb 2012; revised 7 Mar 2012; accepted 8 Mar 2012; published 13 Mar 2012

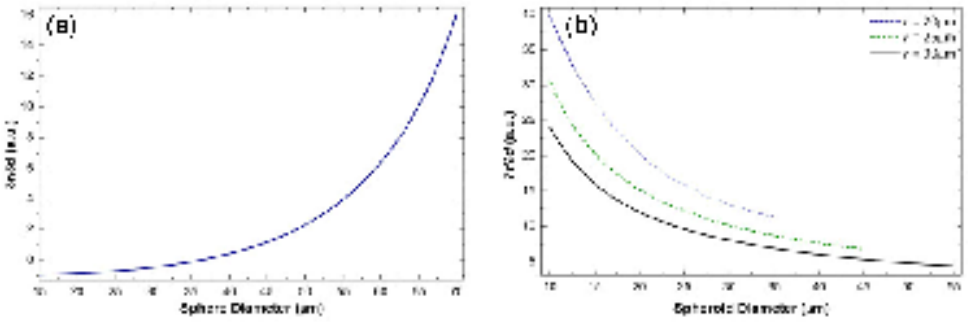

Fig. 2. (a) Theoretical value of $\delta r/\delta d$ as a function of d of a quasi-spherical cavity and (b) an oblate spheroidal cavity for different values of r. In all cases $r > d$.

neglected since γ of an optical fiber made of silica is extremely low (~5.5×10^{-7}/°C). In these circumstances Eq. (1) can be rewritten as:

$$\frac{\delta V}{V} \approx -\frac{E}{K}\varepsilon_a. \tag{2}$$

The total glass volume of the section of optical fiber that contains the cavity is simply the volume of the glass cylinder of radius R and length d minus the volume of the cavity which depends on the cavity size and shape. In the case of an oblate spheroidal cavity of size $2d$x$2r$ the quoted volume can be expressed as:

$$V = \pi d R^2 - \frac{2}{3}\pi r^2 d. \tag{3}$$

The volumetric changes δV can be obtained by simply differentiating Eq. (3). By substituting V and δV, $\varepsilon_a = \delta d/d$ and neglecting changes in fiber radius (i.e., $\delta R \approx 0$) we arrive to the following expression:

$$\frac{\delta r}{\delta d} = \frac{3}{4}\left(\frac{E}{K}+1\right)\left(\frac{R^2}{r^2}-\frac{2}{3}\right)\frac{r}{d}. \tag{4}$$

Thus, $\delta\lambda_m$, hence the sensitivity of a FPI with spheroidal cavity, depends on r and d. It is not difficult to show that $\delta r/\delta d$ depends also on r, d, or on both, when the cavity of the FPI has other shapes, let us say spherical or cylindrical ones.

3. Results and discussion

In Fig. 2 we plot the term $\delta r/\delta d$ as a function of d considering a quasi-spherical cavity ($r \approx d$) and a spheroidal one. In the latter case, three values of r were assumed, but in all cases $r > d$. The optical fiber radius R, the silica Young's (E) and bulk (K) modulus were assumed to be, respectively, 62.5 μm, 70.3 GPa and 36.8 GPa. Note from the figure that when the cavity has spheroidal shape the term $\delta r/\delta d$ increases as the cavity becomes smaller. However, the opposite occurs when the cavity has spherical shape. In a practical situation neither d nor r can be arbitrary small or large. The values allowed for d and r range between ~10 μm to ~50 μm, *i.e.*, between values that are larger than the core diameter but smaller than the radius of a stan-

#162708 - $15.00 USD Received 8 Feb 2012; revised 7 Mar 2012; accepted 8 Mar 2012; published 13 Mar 2012

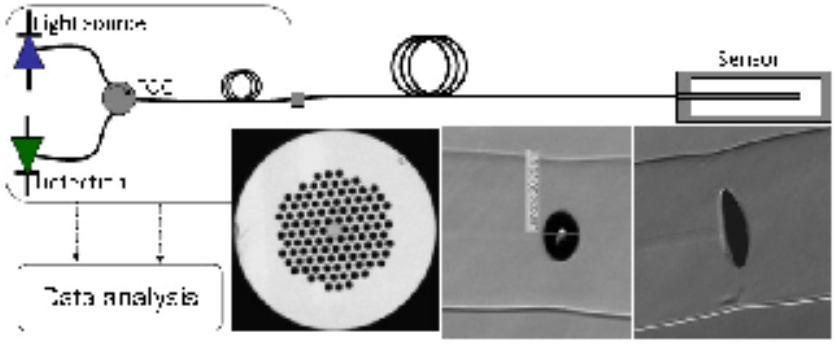

Fig. 3. Schematic diagram of the interrogation set-up. FOC stands for fiber optic circulator. The micrographs show the PCF cross section and two spheroidal cavities with different sizes.

Table 1.

	Prefusion Time	Prefusion arc	Gap	Overlap	Fusion time1	Fusion current 1	Fusion time 2	Fusion current 2	Fusion time 3	Fusion current 2
SMF	0.2s	10.0mA	50.0μm	10.0μm	0.3 s	10.5mA	2.0s	16.3mA	2.0s	12.5mA
FPI	0.3 s	13.0mA	50.0μm	5.0 μm	0.3 s	12.0mA	1.5s	12.5mA	1.5s	12.0mA

dard single mode optical fiber. The results shown in Fig. 2 suggest that the sensitivity of a FPI can be controlled with the shape and dimensions of the cavity. The theoretical analysis here presented is consistent with the experimental results reported in [15], where it was demonstrated that FPIs with larger spherical cavities exhibited higher strain sensitivities. Note also that FPIs with spheroidal cavities are more appealing for optical sensing since the sensitivity can be tailored with an adequate combination of r and d.

To fabricate FPIs with spheroidal cavities we fusion spliced an SMF to a PCF whose cross section is shown in Fig. 3. The dimensions of the PCF were the following: core size diameter of 12 μm, voids with average diameter of 5.6 μm, pitch of 7.5 μm and outer diameter of 130 μm. A conventional splicing machine (Ericsson FSU 955) was used. The parameters of our splicing program are shown in Table 1 along with the parameters of the default program set in the machine for splicing SMFs. The PCF was pressurized with pure nitrogen as described in [16]. Under these splicing conditions the PCF air holes collapse completely over a length of a few hundred micrometers and it makes possible the formation of a microscopic air cavity at the SMF-PCF interface [14–16]. Spheroids with large d and r can be achieved by increasing the pressure in the PCF voids during the splicing process [16]. To achieve spheroids with small d and large r we adjusted the overlap between the fibers to compress the spheroids. For example, Fig. 3 shows the micrographs of two spheroids whose sizes ($2d$x$2r$) were ~10x60 μm and ~29x40 μm. We would like to point out that our technique does not allow the fabrication of cavities with any arbitrary shape or dimensions.

To analyze the performance and sensing properties of our FPIs with spheroidal cavities we launched light to the FPI cavity from a broad-band source through a fiber optic circulator, as sketched in Fig. 3. The reflected light was fed to an optical spectrum analyzer. Figure 4 shows the reflection spectra at different strains of a device whose cavity had a size of 10x60 μm. Note the high fringe contrast which reaches 38dB (visibility of 0.99984) and the prominent shift of the peak. The high visibility is due to the short distance the beam travels and also due to the spherical shape of the reflecting surfaces which minimize the diffraction of the beam inside the cavity. The figure also shows the shift of the interference pattern as a function of the applied strain observed in the FPIs with cavities of sizes of 10x60 μm and 29x40 μm. The strain sensitivity of our FPI with large d and small r was found to be 3.5 pm/με, while that

#162708 - $15.00 USD Received 8 Feb 2012; revised 7 Mar 2012; accepted 8 Mar 2012; published 13 Mar 2012

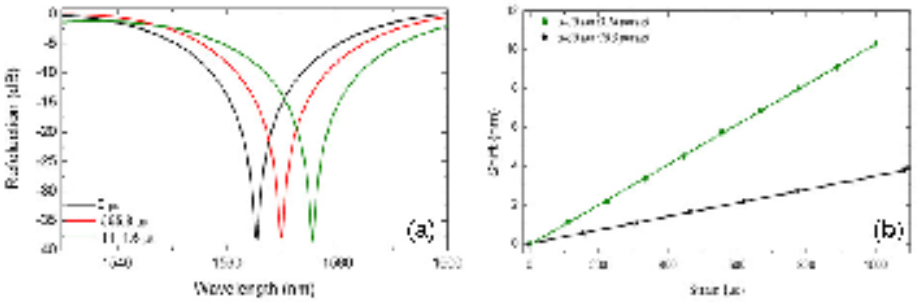

Fig. 4. (a) Reflection spectra at different strains observed in a FPI whose cavity had spheroidal shape and dimensions of 10x60μm. (b) The corresponding shift of the interference pattern as a function of strain is also shown (dots) as well as the shift vs strain observed in a FPI with cavity of 29x40μm (stars).

with small d and large r was ~10.3 pm/με. Again, the results are consistent with the theoretical analysis of spheroidal cavities presented above. The strain sensitivity of our FPI with a 10x60 μm-size spheroidal cavity is circa 10 times higher than that of an FBG [17], and, to the best of our knowledge, higher than that of most low-finesse FPI reported until now. Higher strain sensitivities are theoretically possible, however, with the technique here reported it is not possible to have more control over the spheroid dimensions; nevertheless, it helped us to corroborate the aforementioned theoretical analysis.

The intrinsic temperature sensitivity of FPI with air cavities embedded within the optical fiber is extremely low (~0.95 pm/°C) [5, 15]. This means that the temperature-induced strain error in our FPI with cavity of 10x60 μm is only 0.09 με/°C which is 100 times lower than that of a FBG (~10 με/°C) [17]. Thus, a temperature change of 100°C would be needed to induce an error of only 9 με; therefore, temperature compensation may not be necessary. However, in practical applications the FPI will be packaged and mounted on an object or surface. In these cases the temperature-sensitivity will be governed by the thermal expansion of such an object or surface.

4. Potential applications

The microscopic dimensions of our FPIs along with their low thermal sensitivity and high strain sensitivity can be advantageous for sensing physical parameters of practical interest.

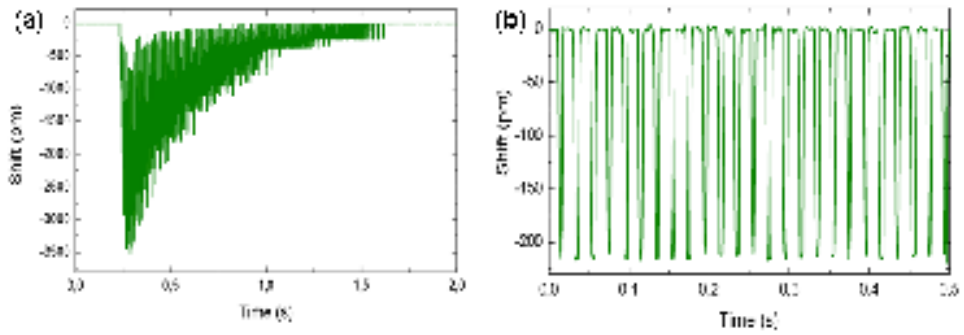

Fig. 5. Shift of the interference pattern as a function of time when a hammer blow (a) and periodic vibration (b) was applied to a FPI whose cavity had a size of 10x60μm.

Here, we demonstrate that highly-sensitive vibration sensors can be devised with our interferometers. To do so a FPI was pre-strained and placed inside a 10 cm-long cylindrical metal tube whose inner/outer diameters were 250/1000 μm. The protected interferometer was then secured on a metallic frame as shown in Fig. 3, thus dynamic strain caused by vibrations could induce a shift of the interference pattern. A hammer blow was applied to the frame,

#162708 - $15.00 USD Received 8 Feb 2012; revised 7 Mar 2012; accepted 8 Mar 2012; published 13 Mar 2012

close to the tube end. The shift of the interference pattern was recorded with a FBG interrogator with maximum measurement frequency of ~970 Hz (I-MON 512E, Ibsen Photonics). The recorded signal is shown in Fig. 5(a). It can be seen that the shift is more prominent immediately after the hammer blow and decreases with time as the vibration is damped. In a second experiment our packaged FPI was placed in close contact with a metallic piece which was subjected to periodic vibration caused by a motor. The recorded signal is shown in Fig. 5(b). Note that both signals presented in the figure are affected by the relatively slow (<1 kHz) speed of the interrogator available for recording these data. However, our interferometer exhibited good performance. It can compete with other optical vibration sensors reported in the literature, see for example [18–21].

The use of our FPIs in real-world applications is promising since miniature, strain and vibration sensors are vital for monitoring structure health, condition in process and production machinery, earthquakes, etc.

5. Conclusions

In conclusion, we have reported on Fabry-Perot interferometers with microcavities embedded in an optical fiber. The theoretical analysis here presented suggests that the shift of the interference pattern, hence the sensitivity of a FPI, depends not only on the separation between the two reflecting surfaces and wavelength but also on the shape and dimensions of the cavity, the diameter of the optical fiber and other constants. To corroborate the theoretical analysis, FPIs with spheroidal shapes were fabricated by fusion splicing a PCF to a SMF with an on-purposed splicing program. High strain sensitivity (~10.3 pm/με) and fringe contrast (~38 dB) were achieved with a FPI whose cavity had spheroidal shape and size of ~10x60 μm. Highly-sensitive vibration sensors were also demonstrated. We believe that the interferometers here proposed are appealing for optical sensing since they exhibit extremely low thermal sensitivity (less than 1 pm/°C), high strain sensitivity, have microscopic size and their fabrication process is really simple.

Acknowledgments

This work was partially supported by the Ministerio de Ciencia e Inovación (Spain) under project TEC2010-14832 and "Ramón y Cajal" fellowship, the Coordenaçao de Aperfeiçoamento Pessoal de Nível Superior (Brazil) under the 251710-8 PhD Fellowship, the Fonds Europeen de Developpement Economique des Regions (FEDER) through the Contrat de Projets Etat Region (CPER) 2007-2013 and also by the Fundació Privada Cellex Barcelona.

#162708 - $15.00 USD Received 8 Feb 2012; revised 7 Mar 2012; accepted 8 Mar 2012; published 13 Mar 2012